

Durham Research Online

Deposited in DRO:

14 January 2015

Version of attached file:

Accepted Version

Peer-review status of attached file:

Peer-reviewed

Citation for published item:

Zeng, Z. and Chen, S. and Selby, D. and Yin, X. and Wang, X. (2014) 'Rhenium–osmium abundance and isotopic compositions of massive sulfides from modern deep-sea hydrothermal systems : implications for vent associated ore forming processes.', *Earth and planetary science letters.*, 396 . pp. 223-234.

Further information on publisher's website:

<http://dx.doi.org/10.1016/j.epsl.2014.04.017>

Publisher's copyright statement:

NOTICE: this is the author's version of a work that was accepted for publication in *Earth and Planetary Science Letters*. Changes resulting from the publishing process, such as peer review, editing, corrections, structural formatting, and other quality control mechanisms may not be reflected in this document. Changes may have been made to this work since it was submitted for publication. A definitive version was subsequently published in *Earth and Planetary Science Letters*, 396, 15 June 2014, 10.1016/j.epsl.2014.04.017.

Additional information:

Use policy

The full-text may be used and/or reproduced, and given to third parties in any format or medium, without prior permission or charge, for personal research or study, educational, or not-for-profit purposes provided that:

- a full bibliographic reference is made to the original source
- a [link](#) is made to the metadata record in DRO
- the full-text is not changed in any way

The full-text must not be sold in any format or medium without the formal permission of the copyright holders.

Please consult the [full DRO policy](#) for further details.

1 **Note:** The sentence being partly modified is in red, and that being newly
2 added are in blue. The contents in black are not changed.

3

4 **Rhenium-osmium abundance and isotopic compositions of massive sulfides from**
5 **modern deep-sea hydrothermal systems: Implications for vent associated ore**
6 **forming processes**

7

8 Zhigang Zeng^{a,*}, Shuai Chen^a, David Selby^b, Xuebo Yin^a, Xiaoyuan Wang^a

9

10

11 ^a Seafloor Hydrothermal Activity Laboratory of the Key Laboratory of Marine
12 Geology and Environment, Institute of Oceanology, Chinese Academy of Sciences,
13 Qingdao 266071, China

14 ^b Department of Earth Sciences, University of Durham, Durham DH1 3LE, UK

15

16

17 *Corresponding author. Email address: zgzenq@ms.qdio.ac.cn (Z.-G. Zeng). Postal
18 address: Seafloor Hydrothermal Activity Laboratory of the Key Laboratory of Marine
19 Geology and Environment, Institute of Oceanology, Chinese Academy of Sciences, 7
20 Nanhai Road, Qingdao 266071, China.

21 Tel.: +86 532 82898525; fax: +86 532 82898525.

22

23 ABSTRACT

24 Studies of rhenium (Re) and osmium (Os) concentrations and isotopic compositions in
25 seafloor hydrothermal sulfides are an important tool for understanding the evolution
26 of hydrothermal systems, allowing the determination of both metal sources and
27 reconstructing the physicochemical conditions of their deposition. The Re-Os
28 concentrations and isotopic compositions of 38 massive sulfide samples have been
29 studied in different hydrothermal fields from the East Pacific Rise (EPR),
30 Mid-Atlantic Ridge (MAR), Central Indian Ridge (CIR), Southwest Indian Ridge
31 (SWIR), and Back-Arc Basin (BAB). The majority of the sulfides possess $^{187}\text{Os}/^{188}\text{Os}$
32 that span a narrow range (1.004 to 1.209), which is most easily explained as a
33 seawater-derived component. This may suggest that those initial $^{187}\text{Os}/^{188}\text{Os}$ isotope
34 compositions of ancient seafloor hydrothermal sulfide deposits which were formed by
35 the mixing process between seawater and hydrothermal fluid, are possible for
36 analysing ancient seawater Os components. Only two of samples
37 (MAR05-TVG1-10-2 and MAR05-TVG1-21 from the Logatchev hydrothermal field
38 (LHF), MAR) possess moderately less radiogenic $^{187}\text{Os}/^{188}\text{Os}$ (0.645 to 0.730), which
39 may reflect the less extent of hydrothermal fluid-seawater mixing during
40 hydrothermal ore-forming process.

41 The rhenium and Os concentrations and $^{187}\text{Re}/^{188}\text{Os}$ ratios of pyrite and Fe-Cu sulfide
42 mineral aggregates (avg Re 11.46 ppb; avg Os 17.76 ppt; avg $^{187}\text{Re}/^{188}\text{Os}$ 11,980.4; n
43 = 24) are usually higher than that of sphalerite or Zn-enriched sulfide mineral
44 aggregate samples (avg Re 0.31 ppb; avg Os 7.09 ppt; avg $^{187}\text{Re}/^{188}\text{Os}$ 206.99; $n = 9$),

suggest that Re and Os are more likely to be incorporated into Fe- and Fe-Cu sulfide mineral facies. A significant positive correlation is observed between Os/Re ratios and Pb concentrations in the sulfide samples from the Edmond hydrothermal field (EHF), whereas Pb-enriched of sulfide is characteristic of low-temperature paragenetic association, suggesting that Os enriched under low-temperature ($< 200^{\circ}\text{C}$) condition. In addition, our Re-Os data are used to estimate that modern seafloor sulfide deposits contain roughly 0.6 to 44 tonnes (avg 4 tonnes, $n = 38$) of Re, and 1 to 48 kg (avg 8 kg, $n = 38$) of Os. The Os flux of global low-temperature hydrothermal fluids to vents is about 11 kg per year, and the excess Os (i.e. Os not incorporated in sulfides) may be carried and become bound in metalliferous sediment, Fe-Mn crusts and nodules distal to the hydrothermal vents.

Keywords: Re-Os isotopes; massive sulfides; seafloor hydrothermal systems

1. Introduction

The study of ore-forming processes of metals is a key to understand the formation, distribution, type, and size of seafloor sulfide deposits (e.g. Baker and German, 2004; Fouquet, 1997; Hannington et al., 2005, 2011; Rona, 2003). The strongly siderophile and chalcophile (i.e. easily dissolved in iron-rich and/or sulfur-rich liquids) (Shirey and Walker, 1998) nature of both Re and Os means these elements are often incorporated directly into sulfide phases. As a result Re-Os isotopic compositions of seafloor massive sulfides provide information about the sources of metal and ore-forming conditions (e.g. Brüggmann et al., 1998; Morelli et al., 2004; Ravizza et al., 1996). To date, the Re and Os distribution and isotope composition in massive sulfides has been determined for some ancient volcanic-hosted massive sulfide (VHMS) deposits in the Iberian Pyrite Belt (Mathur et al., 1999; Munhá, 2005), Southern Urals (Gannoun et al., 2003; Tessalina et al., 2008), Sanbagawa metamorphic belt (Nozaki et al., 2010, 2013), Red Dog deposit of the Brooks Range belt (Morelli et al., 2004), Kuroko ore deposits of the Hokuroku District (Terakado, 2001a), Wanibuchi Mine (Terakado, 2001b), Gacun deposit of southwestern China (Hou et al., 2003), and modern Trans-Atlantic Geotraverse (TAG) hydrothermal field on the MAR (Brüggmann et al., 1998; Ravizza et al., 1996). In the Iberian Pyrite Belt, calculated initial $^{187}\text{Os}/^{188}\text{Os}$ values are ~ 0.37 , which suggest that the continental margin sediments or the volcanic rocks are plausible sources for ore-forming metals (Mathur et al., 1999). In the Southern Urals, Russia, Re concentrations are quite homogenous throughout the hydrothermal system (10 to 30 ppb); however the Os

89 concentrations increase upwards in the hydrothermal system (98 to 1,000 ppt), which
90 could be explained by progressive leaching of Os by high-temperature fluid and its
91 re-deposition (Tessalina et al., 2008). Further, the Os isotopic compositions in Urals
92 ore facies (including massive sulfide) is controlled by the mixture of hydrothermal
93 fluid and seawater (Tessalina et al., 2008), with the majority of Os in the massive
94 sulfides being derived from the submarine high-level mantle rocks (Gannoun et al.,
95 2003). The Sanbagawa metamorphic belt of southwest Japan, hosts numerous
96 Kimmeridgian Iimori Besshi-type deposits for which sulfide minerals possess a wide
97 range of $^{187}\text{Os}/^{188}\text{Os}$ values (~ 0.10 to 0.67 ; Nozaki et al., 2013). The more radiogenic
98 initial $^{187}\text{Os}/^{188}\text{Os}$ values for sulfides from the Iimori Besshi-type are suggested to be
99 caused by the entrainment of contemporaneous seawater with a more radiogenic
100 $^{187}\text{Os}/^{188}\text{Os}$ value into the pristine hydrothermal fluid (Nozaki et al., 2013), which is
101 also proposed for the modern TAG hydrothermal field (0.56 – 1.05 ; Brüggmann et al.,
102 1998). In the Brooks Range belt, Re-Os data of 10 massive and vein pyrites from Red
103 Dog deposit yields an isochron age of 338.3 ± 5.8 Ma with an initial $^{187}\text{Os}/^{188}\text{Os}$ of
104 0.20 ± 0.21 , which differs from the contemporaneous value (~ 1) of seawater (*pers.*
105 *comm.*, Slack, 2014; paper in review to SEG). This indicates that only crustal sources
106 older than ~ 410 Ma are unlikely to provide Os in the ore-forming hydrothermal fluids,
107 and that the unradiogenic value does not preclude a mantle-like source (Morelli et al.,
108 2004). In the Hokuroku District of Japan, sulfides from four Kuroko, three Oko and
109 one Keiko ores from the Kuroko ore deposits yield an isochron age of 14.32 ± 0.51
110 Ma, with an initial $^{187}\text{Os}/^{188}\text{Os}$ value of ~ 0.75 (Terakado, 2001a). This value is in the

111 range of the Miocene seawater $^{187}\text{Os}/^{188}\text{Os}$ value (0.73 to 0.85; Peucker-Ehrenbrink et
112 al., 1995), suggesting that the Os of the Kuroko ore deposits in the northeast Japan
113 was mainly derived from seawater (Terakado, 2001a). In the Wanibuchi Mine (yields
114 an isochron age of 18.44 ± 0.60 Ma), the initial $^{187}\text{Os}/^{188}\text{Os}$ ratio (0.621 ± 0.013)
115 might reflect the contemporaneous local seawater ratio ($\sim 0.57\text{--}0.66$) that was more
116 affected by Os derived from the volcanic activities of Japan Sea formation (Terakado,
117 2001b). In the late Triassic Gacun volcanogenic massive sulfide deposit, southwestern
118 China, the Re-Os isotopic compositions of sulfide ores yield a 8-point isochron age of
119 217 ± 28 Ma, with an initial $^{187}\text{Os}/^{188}\text{Os}$ of 0.52 ± 0.73 , suggesting a mixing of
120 hydrothermal fluid and late Triassic seawater (Hou et al., 2003). The radiogenic Os
121 compositions (0.566–1.054) of sulfide samples from the TAG hydrothermal field
122 indicate that there is a variable mixing of ocean crust-derived Os and seawater Os, and
123 this mixing is controlled by the redox conditions (Brügmann et al., 1998; Ravizza et
124 al., 1996). Although the Re-Os isotopic composition of seafloor hydrothermal sulfides
125 can provide important information on metal and fluid sources, mixing between
126 hydrothermal fluid and seawater, and geochemical processes, little is known about the
127 Re-Os isotopic composition of sulfides from seafloor hydrothermal systems in
128 mid-ocean ridge (MOR) and back-arc basin (BAB), due to their low concentrations
129 ($\text{Re} < 0.2$ ppb; $\text{Os} < 2$ ppt) in sulfides and the difficulty in obtaining pure sulfide
130 samples (e.g. fine-grained intergrowth and the removal of other minerals such as
131 sulfates and oxides). At present, analytical techniques developed by Birck et al. (1997)
132 have allowed precise measurements of Os at a few tens of parts per trillion (ppt) levels,

enabling the analysis of more common sulfide samples (Gannoun et al., 2003).

In this study, Re-Os abundance and isotopic compositions have been measured, for the first time, in the seafloor massive sulfide samples from the **EPR near 13°N and 1-2°S, MAR, CIR, SWIR and BAB** (Fig. 1). We describe the characteristics of Re-Os abundance and isotopic composition in sulfides, in combination with major elements of sulfide samples, characterize the seawater Os contributions, **attempt to** understand the implications of initial $^{187}\text{Os}/^{188}\text{Os}$ for ancient seafloor hydrothermal sulfide deposits, reveal the enrichment condition of Re-Os, and evaluate the Os flux from hydrothermal fluid to seafloor hydrothermal precipitation.

2. Sampling and methods

In 2005, 2007, 2008, 2009, and 2010, during the DY105-17, DY115-19, DY115-20, and DY115-21 cruises of R/V *Dayang Yihao*, sulfide samples were recovered by TV-grab samplers from several sites. These included the fast-spreading EPR near 13°N; the ultra-fast spreading EPR near 1-2°S; the Kairei hydrothermal field (KHF) and Edmond hydrothermal field (EHF) on the intermediate-spreading CIR near 25°S; the A area on the ultra-slow spreading SWIR; and the LHF on the slow-spreading MAR. Sulfide samples from Sonne 99 hydrothermal field (S99HF) in the back-arc North Fiji Basin (NFB) were collected in 1998 during the SO134 cruise of the R/V *Sonne* for the German HYFIFLUX II project (Fig. 1).

In the EPR near 13°N and 1-2°S, KHF, EHF, A area, and S99HF, the massive sulfide deposits are hosted by mid-ocean ridge basalts (MORBs). In the LHF, the massive sulfide deposit is associated with ultramafic rocks located in a debris flow consisting of heterogeneous ultramafic and mafic intrusive rocks, including serpentinized harzburgite, serpentinized dunite, gabbro-norite, and olivine-bearing basalt (Petersen et al., 2009). Massive sulfide deposits include both focused high-temperature (> 300°C) fluid outflow through chimneys as well as low-temperature (< 200°C) fluids from mounds in the EPR near 13°N, KHF, EHF, LHF, and S99HF (Gallant and Von Damm, 2006; Koschinsky et al., 2002; Merlivat et al., 1987; Michard et al., 1984; Petersen et al., 2009). Table 1 and Fig. 2 contain information about the sampling location, depth, and mineralogy of the massive sulfide samples. Most massive sulfide samples indicating multi-stage deposition consist of major pyrite ± marcasite, chalcopyrite,

sphalerite, and minor barite, Pb-sulfide or galena.

Massive sulfide samples were carefully taken from distinct zones or representative portions of the sulfides. All of the samples were crushed and sieved to select sulfide grains between 50 μm and 2 mm, and then sulfides and some gangue minerals were separated by ethanol elutriation. As most of the samples were fine-grained and intergrown, we used an integrated mechanical separating method (including a high-frequency dielectric splitter, a magnetic separator, and an electromagnetic separator) to obtain ~200–500 mg of pure monomineralic or mineral aggregate samples. All sulfide mineral samples for Re-Os analysis were then hand-picked carefully under a binocular microscope to avoid sulfates and oxides. In oxidizing conditions, Re is highly soluble (Crusius et al., 1996), and the seawater-derived hydrogenous Os can be scavenged by Fe-oxides (Ravizza et al., 1996), and Pierson-Wickmann et al. (2002) also showed that Os liberated during alteration was partially re-precipitated in oxides, with Os isotope compositions very similar to those of the original rocks. Whereas, a large amount of Re can be lost during alteration processes (Peucker-Ehrenbrink and Hannigan, 2000). As such, it is possible that the post-depositional oxidation can affect the Re and Os abundances and isotope composition of primary sulfide (e.g. Brüggmann et al., 1998; Gannoun et al., 2003; Ravizza et al., 1996). As a result we took care to avoid the effects of oxidation.

These samples were divided into sub-samples, which were placed in distilled water, exposed to ultrasonic waves for 15min, and then washed in de-ionised Milli-Q water (18.2 M Ω) to remove impurities from the surface. The samples were dried at 65 and

199 105°C and then ground to < 63 µm.

200

201

202

203

204

205

206

207

208

209

210

211

212

213

214

215

216

217

218

219

220

2.1. Fe, Cu, Pb and Zn determinations

Exactly 40mg of the < 200 µm powders were weighed, then added to Teflon vials. Next, 0.5 mL of 22.5 mol/L pure HF, 2 mL of 12 mol/L pure HCl were added in turn and the samples were heated at 150°C for 24h in closed vials on an electrothermal plate. After that, 0.6 mL of 16 mol/L pure HNO₃ was added and heated in closed vials at 150°C for 12h. Then samples were dried until no white smoke was present. When the samples were dry, 1mL of 16 mol/L pure HNO₃ and 1mL de-ionised Milli-Q water (18.2 MΩ) were added to re-dissolve for 12h (Yin et al., 2011). All acids above are MOS (Metal-Oxide-Semiconductor) pure grade. Finally, Fe, Cu, Pb, and Zn were analyzed by IRIS Intrepid II XSP ICP-AES (Thermo Fisher Scientific) at Qingdao Institute of Marine Geology, relative standard deviation (RSD) < 2%. The reference materials GBW07267, GBW07268, GBW07270, and WMS-1A were run as external standards to evaluate the accuracy.

2.2. Rhenium-Osmium Analysis

Rhenium and Os abundance and isotope analyses were performed in the TOTAL Laboratory for Source Rock Geochronology and Geochemistry (a member of the Durham Geochemistry Centre) at Durham University, following standard protocols (Selby et al., 2009). In brief, rhenium and osmium were purified from the sulfide samples (~400 mg) using carius tube digestion with HCL-HNO₃ medium, with the Os isolated and purified using solvent extraction and micro-distillation. Rhenium was separated using anion chromatography. Isotope ratios of Re and Os were determined using negative thermal ionization mass spectrometry on a Thermo Fisher Scientific TRITON mass spectrometer. Analytical blanks (2.5 ± 0.06 pg and 0.2 ± 0.1 pg; 1σ , $n = 3$; respectively for Re and Os, with an average $^{187}\text{Os}/^{188}\text{Os}$ ratio of 0.25 ± 0.03) and results for standard in-house solutions run during this study are identical to those previously published ($^{185}\text{Re}/^{187}\text{Re} = 0.598251 \pm 0.001510$, 1σ S.D., $n = 13$; $^{187}\text{Os}/^{188}\text{Os}$ ratio 0.160912 ± 0.000559 , 1σ , $n = 13$) (Nowell et al., 2008; Selby et al., 2009). Uncertainties for $^{187}\text{Re}/^{188}\text{Os}$ and $^{187}\text{Os}/^{188}\text{Os}$ are determined by full error propagation of uncertainties in Re and Os mass spectrometer measurements, blank abundances and isotopic compositions, spike calibrations and reproducibility of standard Re and Os isotopic values.

3. Results

3.1. Re and Os concentrations in sulfides

Rhenium and Os concentrations and isotopic data are shown in Table 2. Massive sulfides from the EPR near 13°N and 1-2°S, MAR, CIR, SWIR, and BAB have Os concentrations between 1.7 and 79.9 ppt and Re concentrations between 0.10 and 73.60 ppb (Table 2; Figs. 3a, 3b). The Re concentrations in the S99HF are variable (0.10 to 73.60 ppb), and show the largest range, which exhibit two highest concentrations (44.45 and 73.60 ppb) and one lowest concentration (0.10 ppb) in the massive sulfide samples (Table 2). The Os concentrations of sulfide samples from the EHF is significantly more variable (1.7 to 79.9 ppt) than that of sulfide samples from the other hydrothermal fields, if we exclude the three samples (IR05-TVG12-8-2, IR05-TVG13-9.2-1, and 19III-S18-TVG9), the remaining samples do not exhibit much variability (1.7 to 8.84 ppt) (Table 2). The Os concentrations of sulfide samples from the EPR near 13°N consist also a large range (5.74 to 53.36 ppt). Further, Re concentrations of pyrite and Fe-Cu sulfide mineral aggregate samples are usually higher than that of sphalerite or Zn-enriched sulfide mineral aggregates in massive sulfide samples (Table 1, 2; Fig. 4a). The overall ranges in Os contents in massive sulfide samples from the EPR near 13°N and 1-2°S, LHF, EHF, KHF, A area, and NFB are roughly similar (Table 2; Fig. 3a).

3.2. Re-Os isotopic compositions of the sulfides

The measured $^{187}\text{Os}/^{188}\text{Os}$ value in the sulfide samples varied from 0.645 to 1.209 (Table 2), with no relationship shown between $^{187}\text{Os}/^{188}\text{Os}$ ratio and mineral aggregate type (e.g. Fe-sulfide, Fe-Cu sulfide, Zn-rich sulfide) (Fig. 4c). The $^{187}\text{Os}/^{188}\text{Os}$ ratios of all samples are significantly more radiogenic than that of MORB (Fig. 3c). Most of the $^{187}\text{Os}/^{188}\text{Os}$ ratios agree with or are slightly less radiogenic than the value for modern seawater (~ 1.06), which is similar to that estimated for seawater ~ 2 ka (Peucker-Ehrenbrink and Ravizza, 2000) (Fig. 3c). Only two samples possess $^{187}\text{Os}/^{188}\text{Os}$ ratios that are significantly lower than that of seawater (0.645 ± 0.066 , MAR05-TVG1-10-2, and 0.730 ± 0.066 , MAR05-TVG1-21 from the LHF, MAR) (Fig. 3c).

The sulfide samples have a significantly large range of $^{187}\text{Re}/^{188}\text{Os}$ ratios (from 64 to 100,334) (Fig. 3d), although ^{187}Os ingrowth could change the $^{187}\text{Os}/^{188}\text{Os}$ ratios of the sulfide samples during a relatively short interval of time (Brügmann et al., 1998), the young age (e.g. 1,900–2,100 yr, sulfides of the EPR near 13°N ; Lalou et al., 1985) of sulfides precludes any notable ^{187}Os ingrowth despite the large $^{187}\text{Re}/^{188}\text{Os}$ ratios (e.g. sample EPR05-TVG2-1-1 and EPR05-TVG2-1-6). The rather constant $^{187}\text{Os}/^{188}\text{Os}$ values in most samples with very different Re/Os ratios also show insignificant ^{187}Os ingrowth (Brügmann et al., 1998; Table 2). For example, for the most Re enriched sample (42GTV-3, 73.6 ppb Re) only 1.8 ppq ^{187}Os would be generated in ~ 2 ka. In addition, $^{187}\text{Re}/^{188}\text{Os}$ ratios of pyrite and Fe-Cu sulfide mineral aggregates in the massive sulfide samples are usually higher than that of sphalerite or Zn-enriched

309 sulfide mineral aggregate samples (Fig. 4d).

310

311

312

313

314

315

316

317

318

319

320

321

322

323

324

325

326

327

328

329

330

4. Discussion

4.1. Seawater osmium contributions

It is known that the Os isotopic composition of MORB is about 0.133 (Gannoun et al., 2007; Schiano et al., 1997), and is about 0.121 in abyssal peridotite (Harvey et al., 2006; Snow et al., 1995). The $^{187}\text{Os}/^{188}\text{Os}$ ratios of hydrothermal fluids from the Juan de Fuca Ridge are from ~0.110 to 1.04 (Sharma et al., 2000, 2007), which are between MORB (~0.133) and seawater (~1.06). The Os isotopic ratio of present-day and ~ 2 ka seawater is radiogenic (~ 1.0; Peucker-Ehrenbrink and Ravizza, 2000), significantly different from unradiogenic Os isotopic compositions of MORB and ultramafic rocks (e.g. Roy-Barman and Allègre, 1994). Therefore, the Os isotopic compositions of massive sulfides can be used as evidence for the source of osmium and by inference the associated metals (Fe, Cu, Zn) as well as the physicochemical processes involved during metal mobilization (Brügmann et al., 1998).

The majority of the $^{187}\text{Os}/^{188}\text{Os}$ values for the massive sulfide samples fall in a narrow range (0.968–1.209) (Fig. 3c, 5), that are close to or within uncertainty of the modern seawater $^{187}\text{Os}/^{188}\text{Os}$ value (~ 1.06; Peucker-Ehrenbrink and Ravizza, 2000), and significantly more radiogenic than that of MORB (Fig. 3c, 5). All the Os isotopic data in sulfide samples from the EPR near 13°N and 1-2°S, KHF, EHF, A area, and S99HF indicates that the Os is mainly derived from seawater (Fig. 5b), which can be interpreted as evidence of entrainment of seawater into hydrothermal fluids (e.g. Ravizza et al., 1996; Roy-Barman and Allègre, 1994).

In the ancient VMS deposits, initial $^{187}\text{Os}/^{188}\text{Os}$ isotope compositions vary greatly

353 even in the same deposit. Take the Iberian Pyrite Belt for example, initial osmium
354 isotope ratios of pyrites in sulfide-rich stockwork ores are from 0.451 to 1.08, much
355 lower than those in pyrites from cassiterite-rich stockwork ores (4.89 to 7.85), and let
356 alone massive copper-tin ores (0.376 to 14.1) (Mathur et al., 1999; Munhá et al.,
357 2005). The high initial $^{187}\text{Os}/^{188}\text{Os}$ ratios were interpreted to be affected by late
358 hydrothermal and Variscan metamorphic isotope disturbances (Munhá et al., 2005),
359 making the ratios **inappropriate** for tracing of the ancient contemporaneous seawater
360 composition. However, the initial $^{187}\text{Os}/^{188}\text{Os}$ ratio (0.49 ± 0.07) of Neves-Corvo
361 sulfide-rich stockwork ores in the Iberian Pyrite Belt, obtained according to best-fit
362 calculations on the isochron (358 ± 29 Ma) (Munhá et al., 2005) is **nearly identical** to
363 that inferred for Late Devonian (358 ± 9 Ma) seawater ($\sim 0.3\text{--}0.7$; Harris et al., 2013).
364 Further, **the Os isotopic composition of Middle Devonian Givetian (~ 385 Ma)**
365 seawater is estimated to be the same as the initial Os isotopic ratio of Devonian
366 seafloor metalliferous sediments ($^{187}\text{Os}/^{188}\text{Os} \sim 0.17\text{--}0.2$) in the Southern Urals,
367 which **is** associated with Alexandrinka sulfide deposit (Harris et al., 2013; Tessalina et
368 al., 2008). **In the Sanbagawa metamorphic belt, the Re-Os isotopic compositions of**
369 **massive sulfides from the Iimori Besshi-type deposit, yield a model isochron age**
370 **(148.4 ± 1.4 Ma) and an initial $^{187}\text{Os}/^{188}\text{Os}$ of 0.41 ± 0.14 (Nozaki et al., 2013), which**
371 **is similar** to the $^{187}\text{Os}/^{188}\text{Os}$ ratios of ancient seawater which recorded by the
372 individual organic-rich mudstones (ancient seawater age 155 ± 4.3 Ma, initial
373 $^{187}\text{Os}/^{188}\text{Os}$ of 0.59 ± 0.07 ; Cohen et al., 1999), suggesting that these ancient sulfide
374 deposits were formed by the mixing process between ancient seawater and

375 hydrothermal fluid, and their initial $^{187}\text{Os}/^{188}\text{Os}$ ratios were not altered by later
376 hydrothermal fluids or metamorphism after a long geologic period. If it is true, the
377 initial Os isotopic ratios of ancient sulfide deposits can be used in discussion of the
378 origin of Os and by inference the associated metals.

379 The Os isotope composition of seawater has varied through time (Peucker-Ehrenbrink
380 and Ravizza, 2012). Although the Paleozoic record is poorly established, the Cenozoic
381 record shows a progressive trend towards radiogenic values. If seafloor sulfides
382 predominantly record seawater values of Os then this proposes that ancient deposits
383 will have variable Os.

384 In addition, Os isotopic compositions of at last two samples (0.645 ± 0.066 ,
385 MAR05-TVG1-10-2, and 0.730 ± 0.066 , MAR05-TVG1-21) from the LHF in the
386 MAR are less radiogenic than that of ambient seawater, suggesting it is likely to have
387 been influenced by both radiogenic Os from seawater and unradiogenic Os released
388 by alteration of the MORB and/or the ultramafic rocks (Fig. 5a). According to the
389 mixing trajectories calculated using the method outlined by Langmuir et al. (1978),
390 the mixing curve between the MORBs end member (Os concentration 13.26 ppt,
391 $^{187}\text{Os}/^{188}\text{Os}$ ratio 0.136; Gannoun et al., 2007; Schiano et al., 1997), which are usually
392 considered as the source component of seafloor hydrothermal fluid and seawater (Os
393 concentration 0.01 ppt, $^{187}\text{Os}/^{188}\text{Os}$ ratio 1.06; Peucker-Ehrenbrink and Ravizza, 2000)
394 fits most of the Os data points of massive sulfide samples, with $r_{\text{SB}} = 0.1$ (Fig. 5b).

395 Further, the less radiogenic $^{187}\text{Os}/^{188}\text{Os}$ ratios (e.g. sample MAR05-TVG1-10-2 and
396 MAR05-TVG1-21) indicate that Os derived from alteration of the oceanic crust is

released to hydrothermal fluid in association with mixing process between seawater and fluid (Brügmann et al., 1998; Ravizza et al., 1996), which can be taken place both at vent site and in the sub-seafloor where seawater commonly is entrained within pre-existing sulfide deposit (e.g. hydrothermal mounds, layers, lenses, feeder zones, etc.) (e.g. Rona and Scott, 1993; Zierenberg et al., 1998), and comparing to other sulfides (e.g. EPR near 1-2°S, KHF, S99HF), reflect a relative less proportion of seawater component incorporated into these sulfides during mixing between seawater and hydrothermal fluid.

4.2. *Re-Os enrichment*

Rhenium concentrations of this study are partly lower (0.1 to 73.60 ppb) than that of sulfides from the Iimori Besshi-type massive sulfide deposit (24 to 300 ppb; Nozaki et al., 2010), the Alexandrinka ancient seafloor hydrothermal system (11 to 31 ppb; Tessalina et al., 2008), the Dergamish massive sulfide deposits (6 to 41 ppb; Gannoun et al., 2003), and the Red Dog deposit (0.644 to 383 ppb; Morelli et al., 2004), but similar to those of massive sulfides from the TAG hydrothermal field (2 to > 70 ppb; Brüggmann et al., 1998) and the Ivanovka massive sulfide deposits (0.18 to 6 ppb; Gannoun et al., 2003). The variation in Re content reflects changing temperature, pH, redox conditions and complexing behavior of the hydrothermal fluids, Re is highly soluble in seawater oxidizing conditions (larger amounts of seawater mixing with hydrothermal fluid could cause more oxidized conditions), leading to low Re concentrations in sulfide, whereas under hydrothermal fluid reducing conditions it is less mobile and becomes concentrated in sulfide (e.g. Brüggmann et al., 1998; Keppler, 1996; Xiong and Wood, 1999).

The Os concentrations in massive sulfide samples of this study are general higher (1.7 to 79.9 ppt) than that of massive sulfides from the TAG hydrothermal field (0.04–4.20 ppt; Brüggmann et al., 1998). In comparison to ancient massive sulfides, the Os abundances of sulfides from this study are typically lower than that of the Iimori Besshi-type massive sulfide deposit (224 to 660 ppt; Nozaki et al., 2010), the Alexandrinka ancient seafloor hydrothermal system (69 to 1,071 ppt; Tessalina et al., 2008), the Dergamish and Ivanovka massive sulfide deposits (18 to 2,463 ppt;

Gannoun et al., 2003), and the Red Dog deposit (14 to 3,353 ppt; Morelli et al., 2004).

Because of the great mobility of Os in the high-temperature hydrothermal system (Brüggemann et al., 1998), Os concentrations in sulfide samples from the EPR near 13°N and 1-2°S, MAR, CIR, SWIR, and BAB are general higher than that of the massive sulfides from the TAG hydrothermal field, suggesting the formation temperatures of these sulfides are relatively lower than that of the sulfides from the TAG hydrothermal field ($> 300^{\circ}\text{C}$; Chiba et al., 2001).

In many submarine hydrothermal systems, low-temperature ($< 200^{\circ}\text{C}$), diffusely venting sulfide chimneys are common (e.g. Ames et al., 1993). Sulfide assemblages which were formed at different temperatures have distinct major and trace element compositions, such as Pb, which is enriched in the minor of invisible galena, Pb-As sulfosalts in massive sulfide samples (see Fig. 2), is usually precipitated in the low-temperature, slightly oxidizing conditions during the late or the waning stage of hydrothermal activity (e.g. Fouquet et al., 1996; Kim et al., 2006; Kristall et al., 2006), and are attributed to the weaker HS^{-} complexation at lower temperature (Hannington et al., 1991). The Os/Re ratios of massive sulfides show positive correlations ($R^2 = 0.67, p < 0.01, n = 11$) with Pb (up to 0.15 wt.% concentrations) in the EHF (Fig. 6a), which might also indicate Os incorporated into sulfides under lower temperature conditions, possibly less than 200°C (Hannington et al., 1991).

In massive sulfide samples, very low Re content (< 1 ppb) showed positive correlation with Fe. High Re content (> 10 ppb) showed negative correlation with Fe (Fig. 6b), implying that the Re enrichment is not related to the Fe content of massive sulfides.

Some high-Fe samples (e.g. sample 19III-S18-TVG9, Fe content 43.8 %, and sample IR05-TVG13-9.1, Fe content 38.4 %) had the highest Os content (79.9 ppt) and some had the lowest Os content (1.7 ppt) (see Table 2). This tends to imply, judging from these samples, that the Os contents of these massive sulfides are not primarily controlled by the Fe content. Massive sulfide samples with very low Re contents (< 0.2 ppb) have very low Cu contents. Samples with intermediate Re contents (0.2 to 5 ppb) have a wide range of Cu content. Samples with high Re contents (> 5 ppb) also show a significant range of Cu content (Fig. 6c). On the other hand, massive sulfide samples with lower Re concentration usually have higher Zn concentration (Fig. 6d), and Os/Re ratios are high in the Zn-enriched sulfide mineral aggregate samples (e.g. sample 26.1GTV-1, IR05-TVG12-8-3 and IR05-TVG12-14). This also indicates that Re is less compatible than Os in sphalerite or Zn-enriched sulfide mineral aggregate samples, and together these suggest that the Re-Os enrichment is not related to Zn-enriched sulfide mineral facies. This phenomenon is also observed in ancient VMS deposit such as the Red Dog deposit with the higher Re and Os content of pyrite than sphalerite in the massive sulfides (Morelli et al., 2004).

In addition, the high Os contents of sulfides from the Alexandrinka, the Dergamish and Ivanovka massive sulfide deposits in island-arc environment show that the ^{187}Os enrichment of the sulfides from ^{187}Re decay (Brügmann et al., 1998; Tessalina et al., 2008), and the estimated minimal Os contents of Devonian fluid (20 ppt; Tessalina et al., 2008) are three orders of magnitude higher than that ($1.9\text{--}98\times 10^{-3}$ ppt; Sharma et al., 2000, 2007) of the hydrothermal fluid from the Juan de Fuca Ridge in mid-ocean

ridge setting, suggesting that seafloor hydrothermal massive sulfides from MOR (e.g. EPR near 13°N and 1-2°S, CIR, and MAR) are characterized by low Os concentrations compared with island-arc hosted VHMS deposits (e.g. Urals, Iberian pyrite belt; Tessalina et al., 2008). In contrast to the seafloor hydrothermal massive sulfides (Fig. 3a, 3b), the MORBs are depleted in Re and Os which might explain the higher $^{187}\text{Re}/^{188}\text{Os}$ ratios of the sulfides from the EPR near 1-2°S and the KHF, since an increasing $^{187}\text{Re}/^{188}\text{Os}$ ratio shows the interaction of oxidized seawater and reduced hydrothermal fluid. The higher Os and Re concentrations in these samples may reflect that Os and Re were concentrated in the fluid, Os and Re behaves as a highly mobile element during basalt-fluid interaction (Brügmann et al., 1998).

4.3. Re-Os Flux

These modern massive sulfide sample analyses allow a meaningful estimate of the magnitude of the hydrothermal Re and Os flux. We present a simple calculation below the premise that vent fluids can readily supply Re and Os with the $^{187}\text{Os}/^{188}\text{Os}$ ratio near the present-day seawater (~ 1.06) to the massive sulfides. The amount of seafloor massive sulfide deposits in the global oceans has been estimated by using new deposit occurrence data from 10,000 km of ridge, arc, and back-arc spreading centers, which is on the order of 6×10^8 tonnes, containing about 3×10^7 tonnes of copper and zinc (Hannington et al., 2011). The method to roughly estimate the seafloor massive sulfide sink for Re and Os:

$$S_{\text{Re}} = M_{\text{sulfide}} \times X_{\text{Re}} \dots \dots \dots (1)$$

$$S_{\text{Os}} = M_{\text{sulfide}} \times X_{\text{Os}} \dots \dots \dots (2)$$

where S_{Re} and S_{Os} are the soluble Re and Os from hydrothermal fluids supplied to the massive sulfide deposits; M_{sulfide} is the total mass of seafloor massive sulfide deposits, as above; and X_{Re} and X_{Os} are the Re and Os contents in the massive sulfide. Based on analyses of Re (0.1–73.60 ppb) and Os (1.7–79.9 ppt) in seafloor massive sulfides from the EPR near 13°N and 1–2°S, MAR, CIR, SWIR, and BAB, it is estimated that roughly 0.6 to 44 tonnes (avg 4 tonnes, $n = 38$) of soluble Re and 1 to 48 kg (avg 8 kg, $n = 38$) of soluble Os from hydrothermal fluids is supplied to the sulfide deposits.

In addition, Os enrichment of seafloor massive sulfide samples from the EPR near 13°N and 1–2°S, LHF, KHF, EHF, A area, and S99HF is occurring under low-temperature hydrothermal fluid conditions. On the mid-ocean ridges, the mass of

hydrothermal fluid heated to low-temperatures ($< 350\text{ }^{\circ}\text{C}$) is on the order of 6–12 $\times 10^{13}$ kg/yr (Elderfield and Schultz, 1996). Assuming Os concentration of 98 pg/kg in the low-temperature fluids as suggested by Sharma et al. (2000), the global flux of Os to low-temperature hydrothermal vents is about 5–11 kg per year, far less than the 100 kg per year estimated by Ravizza et al. (1996). On these figures, it is seen that in just several years, low-temperature vents at the mid-ocean ridges alone transport more Os to the oceans than is estimated to occur in all of the seafloor low-temperature hydrothermal sulfide deposits from the ocean ridges, arcs and back-arc basins. The fate of the excess Os is unclear, but it has long been known that distal marine sediments, Fe-Mn crusts and nodules are enriched in Os deposited from plumes associated with mid-ocean ridge hydrothermal systems (Burton et al., 1999; Palmer and Turekian, 1986; Ravizza and McMurtry, 1993; Ravizza et al., 1996). This plume fallout does not form seafloor hydrothermal sulfide deposits, and may account for a large fraction of the missing Os.

5. Conclusions

The study of Re-Os systematics of seafloor massive sulfide from the MORs and BAB indicates that the Re concentrations range from 0.1 to 73.6 ppb, Os concentrations are very low, range from 1.7 to 79.9 ppt, and mainly derived from seawater. Two samples from the LHF have shown that Os content and isotopic compositions are controlled by the extent of mixing between hydrothermal fluid and seawater. Since the Os in **most of the** modern seafloor massive sulfide samples being predominantly derived from seawater, it is possible that the initial Os of ancient seafloor sulfide deposits may be also from ancient seawater. Therefore, the initial $^{187}\text{Os}/^{188}\text{Os}$ isotopic ratio of sulfide may be useful in **discussions of** the composition of ancient seawater. **Also, the Re-Os isotopic systematics** may be useful **in speculation about the similarity between ancient sulfide deposit and modern seafloor hydrothermal deposit.**

The enrichment of Os in these seafloor massive sulfides is consistently related to low-temperature ($< 200^{\circ}\text{C}$) venting. **The massive sulfide samples with lower Re contents and higher Os/Re ratios usually have higher Zn contents, indicating that Re is less compatible than Os in sphalerite or Zn-enriched sulfide mineral aggregates.** It is estimated that the seafloor massive sulfide deposits contain **a total of** roughly **0.6–44 tonnes of Re and 1–48 kg of Os.** This implies that it is unlikely that a large Re-Os-type massive sulfide deposit will be discovered in the ocean. In addition, the global flux of Os to low-temperature hydrothermal vents is up to 11 kg per year, **it seems probable that** the excess Os becomes associated with sediments, **Fe-Mn crusts and nodules** distal from the hydrothermal vents.

Acknowledgements

We would like to thank the crews during the DY105-17, DY115-19, DY115-20, and DY115-21 cruises for helping us collect samples. We are grateful to Dr. Erio Rahders of Institute for Geological Sciences, Geology Department, Free University of Berlin, Dr. Xiguang Deng of Guangzhou Marine Geological Survey, China Geological Survey, and Dr. Huaiming Li of Second Institute of Oceanography, SOA, China for providing some of the samples. We are most grateful for the detailed and constructive comments and suggestions provided by Dr. John F. Slack, Dr. Tatsuo Nozaki and one anonymous reviewer, which greatly improved an earlier version of the manuscript. This work was supported by National Key Basic Research Program of China (Grant No. 2013CB429700), National Special Fund for the 12th Five Year Plan of COMRA (Grant No. DY125-12-R-02, DY125-11-R-05), National Natural Science Foundation of China (Grant No. 41325021, 40830849, 40976027), Strategic Priority Research Program of the Chinese Academy of Sciences (Grant No. XDA11030302), and Shandong Province Natural Science Foundation of China for Distinguished Young Scholars (Grant No. JQ200913).

595 **References**

- 596 Ames, D.E., Franklin, J.M., Hannington, M.D., 1993. Mineralogy and geochemistry
597 of active and inactive chimneys and massive sulfide, Middle Valley, northern
598 Juan de Fuca Ridge: An evolving hydrothermal system. *Can. Mineral.* 31,
599 997–1024.
- 600 Baker, E.T., German, C.R., 2004. On the global distribution of mid-ocean ridge
601 hydrothermal vent-fields. *Amer. Geophys. Union, Geophys. Monogr.* 148, pp.
602 245–266.
- 603 Birck, J.-L., Roy-Barman, M., Capmas, F., 1997. Re-Os isotopic measurements at
604 femtomole level in natural samples. *Geostand. Newsl.* 20, 19–27.
- 605 Brügmann, G.E., Birck, J.L., Herzig, P.M., Hofmann, A.W., 1998. Os isotopic
606 composition and Os and Re distribution in the active mound of the TAG
607 hydrothermal system, Mid-Atlantic Ridge. *Proc. ODP, Sci. Res.* 158, 91–100.
- 608 Burton, K.W., Bourdon, B., Birck, J.-L., Allègre, C.J., 1999. Osmium isotope
609 variations in the oceans recorded by Fe-Mn crusts. *Earth Planet. Sci. Lett.* 171,
610 185–197.
- 611 Chiba, H., Masuda, H., Lee, S.-Y., Fujioka, K., 2001. Chemistry of hydrothermal
612 fluids at the TAG active mound, MAR 26°N, in 1998. *Geophys. Res. Lett.* 28,
613 2919–2922.
- 614 Cohen, A.S., Coe, A.J., Bartlett, J.M., Hawkesworth, C.J., 1999. Precise Re-Os ages
615 of organic-rich mudrocks and the Os isotopic composition of Jurassic seawater.
616 *Earth Planet. Sci. Lett.* 167, 159–173.

617 [Crusius, J., Calvert, S., Pedersen, T., Sage, D., 1996. Rhenium and molybdenum](#)
618 [enrichment in sediments as indicators of oxic, suboxic and sulfidic conditions of](#)
619 [deposition. Earth Planet. Sci. Lett. 145, 65–78.](#)

620 Elderfield, H., Schultz, A., 1996. Mid-ocean ridge hydrothermal fluxes and the
621 chemical composition of the ocean. *Annu. Rev. Earth Planet. Sci.* 24, 191–224.

622 Fouquet, Y., Knott, R., Cambon, P., Fallick, A., Rickard, D., Desbruyeres, D., 1996.
623 Formation of large sulfide mineral deposits along fast spreading ridges.
624 Example from off-axial deposits at 12°43'N on the East Pacific Rise. *Earth*
625 *Planet. Sci. Lett.* 144, 147–162.

626 Fouquet, Y., 1997. Where are the large hydrothermal sulphide deposits in the oceans?
627 *Phil. Trans. R. Soc. Lond. A* 355, 427–441.

628 [Gallant, R.M., Von Damm, K.L., 2006. Geochemical controls on hydrothermal fluids](#)
629 [from the Kairei and Edmond vent fields, 23°–25°S, Central Indian Ridge.](#)
630 [Geochem. Geophys. Geosyst. 7, Q06018, doi:10.1029/2005GC001067.](#)

631 Gannoun, A., Tessalina, S., Bourdon, B., Orgeval, J.-J., Birck, J.-L., Allègre, C.-J.,
632 2003. Re-Os isotopic constraints on the genesis and evolution of the Dergamish
633 and Ivanovka Cu (Co, Au) massive sulphide deposits, south Urals, Russia.
634 *Chem. Geol.* 196, 193–207.

635 Gannoun, A., Burton, K.W., Parkinson, I.J., Alard, O., Schiano, P., Thomas, L.E.,
636 2007. The scale and origin of the osmium isotope variations in mid-ocean ridge
637 basalts. *Earth Planet. Sci. Lett.* 259, 541–556.

638 Hannington, M., Herzig, P., Scott, S., Thompson, G., Rona, P., 1991. Comparative

639 mineralogy and geochemistry of gold-bearing sulfide deposits on the mid-ocean
640 ridges. *Mar. Geol.* 101, 217–248.

641 Hannington, M.D., Jonasson, I.R., Herzig, P.M., Petersen, S., 1995. Physical and
642 chemical processes of seafloor mineralization at mid-ocean ridges. In Humphris,
643 S.E., Zierenberg, R.A., Mullineaux, L.S., Thomson, R.E., (eds.), *Seafloor
644 Hydrothermal Systems: Physical, Chemical, Biological and Geological
645 Interactions*, Amer. Geophys. Union, Geophys. Monogr. 91, pp. 115–157.

646 Hannington, M., Jamieson, J., Monecke, T., Petersen, S., Beaulieu, S., 2011. The
647 abundance of seafloor massive sulfide deposits. *Geology* 39, 1155–1158.

648 Harris, N.B., Mnich, C.A., Selby, D., Korn, D., 2013. Minor and trace element and
649 Re-Os chemistry of the upper Devonian Woodford shale, Permian basin, west
650 Texas: Insights into metal abundance and basin processes. *Chem. Geol.*, 356,
651 76–93. <http://dx.doi.org/10.1016/j.chemgeo.2013.07.018>.

652 Harvey, J., Gannoun, A., Burton, K.W., Rogers, N.W., Alard, O., Parkinson, I.J., 2006.
653 Ancient melt extraction from the oceanic upper mantle revealed by Re-Os
654 isotopes in abyssal peridotites from the Mid-Atlantic ridge. *Earth Planet. Sci.
655 Lett.* 244, 606–621.

656 Hou, Z.-Q., Wang, S.-X., Du, A.-D., Qu, X.-M., Sun, W.-D., 2003. Re-Os dating of
657 sulfides from the volcanogenic massive sulfide deposit at Gacun, Southwestern
658 China. *Resour. Geol.* 53, 305–310.

659 Kim, J., Lee, I., Halbach, P., Lee, K.-Y., Ko, Y.-T., Kim, K.-H., 2006. Formation of
660 hydrothermal vents in the North Fiji Basin: Sulfur and lead isotope constraints.

661 [Chem. Geol. 233, 257–275.](#)

662 Keppler, H., 1996. Constraints from partitioning experiments on the composition of
663 subduction zone fluids. *Nature* 380, 237–240.

664 [Koschinsky, A., Seifert, R., Halbach, P., Bau, M., Brasse, S., De Carvalho, L.M.,](#)
665 [Fonseca, N.M., 2002. Geochemistry of diffuse low-temperature hydrothermal](#)
666 [fluids in the North Fiji Basin. *Geochim. Cosmochim. Acta* 66, 1409–1427.](#)

667 Kristall, B., Kelly, D.S., Hannington, M.D., Delaney, J.R., 2006. Growth history of a
668 diffusely venting sulfide structure from the Juan de Fuca Ridge: A petrological
669 and geochemical study. *Geochem. Geophys. Geosyst.* 7, Q07001,
670 doi:10.1029/2005GC001166.

671 Lalou, C., Brichet, E., Hekinian, R., 1985. Age dating of sulfide deposits from axial
672 and off axial structures of the East Pacific Rise near 12°50'N. *Earth Planet. Sci.*
673 *Lett.* 75, 59–71.

674 [Langmuir, C.H., Vocke, R.D.Jr., Hanson, G.N., 1978. A general mixing equation with](#)
675 [applications to Icelandic basalts. *Earth Planet. Sci. Lett.* 37, 380–392.](#)

676 Mathur, R., Ruiz, J., Tornos, F., 1999. Age and sources of the ore at Tharsis and Rio
677 Tinto, Iberian Pyrite Belt, from Re-Os isotopes. *Miner. Deposita* 34, 790–793.

678 [Merlivat, L., Pineau, F., Javoy, M., 1987. Hydrothermal vent waters at 13°N on the](#)
679 [East Pacific Rise: isotopic composition and gas concentration. *Earth Planet. Sci.*](#)
680 [Lett.](#) 84, 100–108.

681 Michard, G., Albarède, F., Michard, A., Minster, J.-F., Charlou, J.-J., Tan, N., 1984.
682 [Chemistry of solutions from the 13°N East Pacific Rise hydrothermal site. *Earth*](#)

683 [Planet. Sci. Lett. 67, 297–307.](#)

684 Morelli, R.M., Creaser, R.A., Selby, D., Kelley, K.D., Leach, D.L., King, A.R., 2004.

685 Re-Os sulfide geochronology of the Red Dog sediment-hosted Zn-Pb-Ag

686 deposit, Brooks range, Alaska. *Econ. Geol.* 99, 1569–1576.

687 Munhá, J., Relvas, J.M.R.S., Barriga, F.J.A.S., Conceição, P., Jorge, R.C.G.S., Mathur,

688 R., Ruiz, J., Tassinari, C.C.G., 2005. Osmium isotope systematics in the Iberian

689 Pyrite Belt. In: Mao, J., Bierlein, F. (Eds.), *Mineral Deposit Research: Meeting*

690 *the Global Challenge*, Springer Berlin Heidelberg, pp. 663–666.

691 Nowell, G.M., Luguet, A., Pearson, D.G., Horstwood, M.A., 2008. Precise and

692 accurate $^{186}\text{Os}/^{188}\text{Os}$ and $^{187}\text{Os}/^{188}\text{Os}$ measurements by Multi-Collector Plasma

693 Ionisation Mass Spectrometry (MC-ICP-MS) part I: solution analyses. *Chem.*

694 *Geol.* 248, 363–393.

695 Nozaki, T., Kato, Y., Suzuki, K., 2010. Re-Os geochronology of the Iimori

696 Besshi-type massive sulfide deposit in the Sanbagawa metamorphic belt, Japan.

697 *Geochim. Cosmochim. Acta* 74, 4322–4331.

698 [Nozaki, T., Kato, Y., Suzuki, K., 2013. Late Jurassic ocean anoxic event: evidence](#)

699 [from voluminous sulphide deposition and preservation in the Panthalassa. *Sci.*](#)

700 [Rep. 3, 1889, doi:10.1038/srep01889.](#)

701 [Palmer, M.R., Turekian, K.K., 1986. \$^{187}\text{Os}/^{186}\text{Os}\$ in marine manganese nodules and the](#)

702 [constraints on the crustal geochemistries of rhenium and osmium. *Nature* 319,](#)

703 [216–220.](#)

704 Petersen, S., Kuhn, K., Kuhn, T., Augustin, N., Hékinian, R., Franz, L., Borowski, C.,

2009. The geological setting of the ultramafic-hosted Logatchev hydrothermal
field (14°45'N, Mid-Atlantic Ridge) and its influence on massive sulfide
formation. *Lithos* 112, 40–56.

Peucker-Ehrenbrink, B., Ravizza, G., Hofmann, A.W., 1995. The marine $^{187}\text{Os}/^{186}\text{Os}$
record of the past 80 million years. *Earth Planet. Sci. Lett.* 130, 155–167.

Peucker-Ehrenbrink, B., Hannigan, R.E., 2000. Effects of black shale weathering on
the mobility of rhenium and platinum group elements. *Geology* 28, 475–478.

Peucker-Ehrenbrink, B., Ravizza, G., 2000. The marine osmium isotope record. *Terra
Nova* 12, 205–219.

Peucker-Ehrenbrink, B., Ravizza, G., 2012. Chapter 8 - Osmium Isotope Stratigraphy.
The Geologic Time Scale, Boston, 145 – 166.
<http://dx.doi.org/10.1016/B978-0-444-59425-9.00008-1>.

Pierson-Wickmann, A.C., Reisberg, L., France-Lanord, C., 2002. Behavior of Re and
Os during low-temperature alteration: Results from Himalayan soils and altered
black shales. *Geochim. Cosmochim. Acta* 66, 1539–1548.

Ravizza, G., McMurtry, G.M., 1993. Osmium isotopic variations in metalliferous
sediments from the East Pacific Rise and the Bauer Basin. *Geochim.
Cosmochim. Acta* 57, 4301–4310.

Ravizza, G., Martin, C.E., German, C.R., Thompson, G., 1996. Os isotopes as tracers
in seafloor hydrothermal systems: metalliferous deposits from the TAG
hydrothermal area, 26°N Mid-Atlantic Ridge. *Earth Planet. Sci. Lett.* 138, 105–
119.

727 Rona, P.A., Scott, S.D., 1993. Seafloor hydrothermal mineralization: New perspective.
728 Econ. Geol. 88, 1935–1976.

729 Rona, P.A., 2003. Resources of the sea floor. Science 299, 673–674.

730 Roy-Barman, M., Allègre, C.J., 1994. $^{187}\text{Os}/^{186}\text{Os}$ ratios of mid-ocean ridge basalts
731 and abyssal peridotites. Geochim. Cosmochim. Acta 58, 5043–5054.

732 Schiano, P., Birck, J.L., Allègre, C.J., 1997. Osmium-strontium-neodymium-lead
733 isotopic covariations in mid-ocean ridge basalt glasses and the heterogeneity of
734 the upper mantle. Earth Planet. Sci. Lett. 150, 363–379.

735 Selby, D., Kelley, K.D., Hitzman, M.W., Zieg, J., 2009. Re-Os sulfide (bornite,
736 chalcopyrite and pyrite) systematics of the carbonate-hosted copper deposits at
737 Ruby Creek, southern Brooks Range, Alaska. Econ. Geol. 104, 437–444.

738 Sharma, M., Wasserburg, G.J., Hofmann, A.W., Butterfield, D.A., 2000. Osmium
739 isotopes in hydrothermal fluids from the Juan de Fuca Ridge. Earth Planet. Sci.
740 Lett. 179, 139–152.

741 Sharma, M., Rosenberg, E.J., Butterfield, D.A., 2007. Search for the proverbial
742 mantle osmium sources to the oceans: Hydrothermal alteration of mid-ocean
743 ridge basalt. Geochim. Cosmochim. Acta 71, 4655–4667.

744 Shirey, S.B., Walker, R.J., 1998. The Re-Os isotope system in cosmochemistry and
745 high-temperature geochemistry. Annu. Rev. Earth Planet. Sci. 26, 423–500.

746 Snow, J.E., Reisberg, L., 1995. Os isotopic systematics of the MORB mantle: results
747 from altered abyssal peridotites. Earth Planet. Sci. Lett. 133, 411–421.

748 Terakado, Y., 2001a. Re-Os dating of the Kuroko ore deposits from the Hokuroku

749 [district, Akita Prefecture, Northeast Japan. J. Geol. Soc. Japan 107, 354–357.](#)

750 Terakado, Y., 2001^b. Re-Os dating of the Kuroko ores from the Wanibuchi Mine,
751 Shimane Prefecture, southwestern Japan. *Geochem. J.* 35, 169–174.

752 Tessalina, S.G., Bourdon, B., Maslennikov, V.V., Orgeval, J.-J., Birck, J.-L., Gannoun,
753 A., Capmas, F., Allègre, C.-J., 2008. Osmium isotope distribution within the
754 Palaeozoic Alexandrinka seafloor hydrothermal system in the Southern Urals,
755 Russia. *Ore Geol. Rev.* 33, 70–80.

756 Xiong, Y., Wood, S., 1999. Experimental determination of the solubility of ReO₂ and
757 the dominant oxidation state of rhenium in hydrothermal solutions. *Chem. Geol.*
758 158, 245–256.

759 Yin, X.B., Zeng, Z.G., Li, S.Z., Wu, L., Wang, X.Y., Zhang, G.L., Chen, S., 2011.
760 Determination of trace elements in sulfide samples by inductively coupled
761 plasma-mass spectrometry. *Chinese J. Anal. Chem.* 39, 1228–1232 ([in Chinese](#)
762 [with English abstract](#)).

763 Zierenberg, R.A., Fouquet, Y., Miller, D.J., Bahr, J.M., Baker, P.A., Bjerkgard, T.,
764 Brunner, C.A., Duckworth, R.C., Gable, R., Geiskes, J., Goodfellow, W.D.,
765 Groschel-Becker, H.M., Guerlin, G., Ishibashi, J., Iturrino, G., James, R.H.,
766 Lackschewitz, K.S., Marquez, L.L., Nehlig, P., Peter, J.M., Rigsby, C.A.,
767 Schultheiss, P., Shanks, W.C.III, Simoneit, B.R.T., Summit, M., Teagle, D.A.H.,
768 Urvak, M., Zuffa, G.G., 1998. The deep structure of a sea-floor hydrothermal
769 deposit. *Nature* 392, 485–488.

770

Figure Captions

Fig. 1. Locations of seafloor massive sulfide samples from deep-sea hydrothermal fields.

Fig. 2. Examples of Fe-Cu-Zn sulfide assemblages in seafloor massive sulfides. (a) Photomicrograph of Fe-rich massive sulfide in sample 113.1GTV-1 showing euhedral pyrite grains and collomorph pyrite. (b) Cu-rich massive sulfide in sample MAR05-TVG1-9. (c) Zn-rich massive sulfide containing minor chalcopyrite and pyrite in sample 26.1GTV1. (d) Back-scattered electron microprobe images of the mineral texture in sample IR05-TVG13-4-2 shows sphalerite that has replaced barite, and sphalerite containing smaller grain of pyrite. (e) Massive pyrite containing Pb-sulfide microcrystallite in sample EPR05-TVG1-2-4. (f) Massive pyrite containing smaller grain of galena in sample 26.2GTV-2. Observations were conducted using a TESCAN VEGA 3 LMH scanning electron microscope. Ba-barite; Sp-sphalerite; Py-pyrite; Cpy-chalcopyrite; Gn-galena.

Fig. 3. (a) Os concentrations, (b) Re concentrations, (c) $^{187}\text{Os}/^{188}\text{Os}$ values, and (d) $^{187}\text{Re}/^{188}\text{Os}$ values in seafloor massive sulfides, hydrothermal precipitates, hydrothermal fluids, hydrothermal plumes, metalliferous sediment, MORBs, peridotites, sulfides in MORBs, and sulfides in peridotites. Seafloor massive sulfide data is from Brüggmann et al. (1998) and Ravizza et al. (1996) and this work.

High-temperature (HT), low-temperature (LT) hydrothermal fluid and hydrothermal plume data are from Sharma et al. (2000, 2007). TAG LT hydrothermal precipitate and metalliferous sediment data are from Ravizza et al. (1996). MORBs and sulfides in MORBs data are from Schiano et al. (1997) and Gannoun et al. (2007). Abyssal peridotite and sulfides in peridotite data are from Snow et al. (1995) and Harvey et al. (2006). Seawater data is from Peucker-Ehrenbrink and Ravizza (2000).

Fig. 4. (a) Re concentrations, (b) Os concentrations, (c) $^{187}\text{Os}/^{188}\text{Os}$ ratios, (d) $^{187}\text{Re}/^{188}\text{Os}$ ratios of different sulfide mineral assemblages from the seafloor massive sulfide samples. Red diamond symbols indicate Re concentrations, Os concentrations, $^{187}\text{Os}/^{188}\text{Os}$ ratios, and $^{187}\text{Re}/^{188}\text{Os}$ ratios of different sulfide mineral assemblages. Blue crosses indicate the average value of Re concentrations, Os concentrations, $^{187}\text{Os}/^{188}\text{Os}$ ratios, and $^{187}\text{Re}/^{188}\text{Os}$ ratios of different sulfide mineral assemblages.

Fig. 5. (a) $^{187}\text{Re}/^{188}\text{Os}$ vs. $^{187}\text{Os}/^{188}\text{Os}$ plot; (b) $^{187}\text{Os}/^{188}\text{Os}$ vs. Os concentration plot. Mixing curves between seawater and MORBs with a mixing parameter $r_{\text{SB}} = [^{188}\text{Os}]_{\text{MORBs}}/[^{188}\text{Os}]_{\text{Seawater}} = 0.1$, which fit most of the Os data of massive sulfides. Mixing curves between seawater and abyssal peridotites with a mixing parameter $r_{\text{SP}} = [^{188}\text{Os}]_{\text{abyssal peridotites}}/[^{188}\text{Os}]_{\text{Seawater}} = 0.1$, which fit some of the Os data of massive sulfides. Mixing curves between seawater and sulfides in MORBs and abyssal peridotites with mixing parameter $r_{\text{SSB}} = [^{188}\text{Os}]_{\text{sulfides in MORBs}}/[^{188}\text{Os}]_{\text{Seawater}} = 0.1$, and $r_{\text{SSP}} = [^{188}\text{Os}]_{\text{sulfides in abyssal peridotites}}/[^{188}\text{Os}]_{\text{Seawater}} = 0.1$, respectively. r reflects the

extent of curvature of the mixing curve (Langmuir et al., 1978). $[^{188}\text{Os}]_{\text{Seawater}}$, $[^{188}\text{Os}]_{\text{MORBs}}$, $[^{188}\text{Os}]_{\text{abyssal peridotites}}$, $[^{188}\text{Os}]_{\text{sulfides in MORBs}}$, and $[^{188}\text{Os}]_{\text{sulfides in abyssal peridotites}}$ are the concentrations of ^{188}Os in seawater, MORBs, abyssal peridotites, sulfides of MORBs, and sulfides of abyssal peridotites.

Fig. 6. Variations of (a) Pb content and Os/Re ratio, (b) Fe content and Re content, (c) Cu content and Re content, and (d) Zn content and Re content in seafloor massive sulfide samples. Re content of massive sulfide samples < 1 ppb, there is a positive correlation between Re and Fe. Re content > 10 ppb, there is a negative correlation between Re and Fe in massive sulfides.

837 **Table 1** Description of seafloor massive sulfide samples.

838

839 **Table 2** Re-Os isotopic compositions of seafloor massive sulfides.

840

Research highlights

- Seawater is a significant source of Re and Os in seafloor massive sulfides
- Initial $^{187}\text{Os}/^{188}\text{Os}$ ratios of ancient sulfides can trace ancient seawater component
- $^{187}\text{Os}/^{188}\text{Os}$ ratios of seafloor massive sulfides is not controlled by mineral facies
- Os is enriched in low-temperature conditions
- Global seafloor sulfide deposits contain roughly 4 tonnes of Re and 8 kg of Os

Figure 1
[Click here to download high resolution image](#)

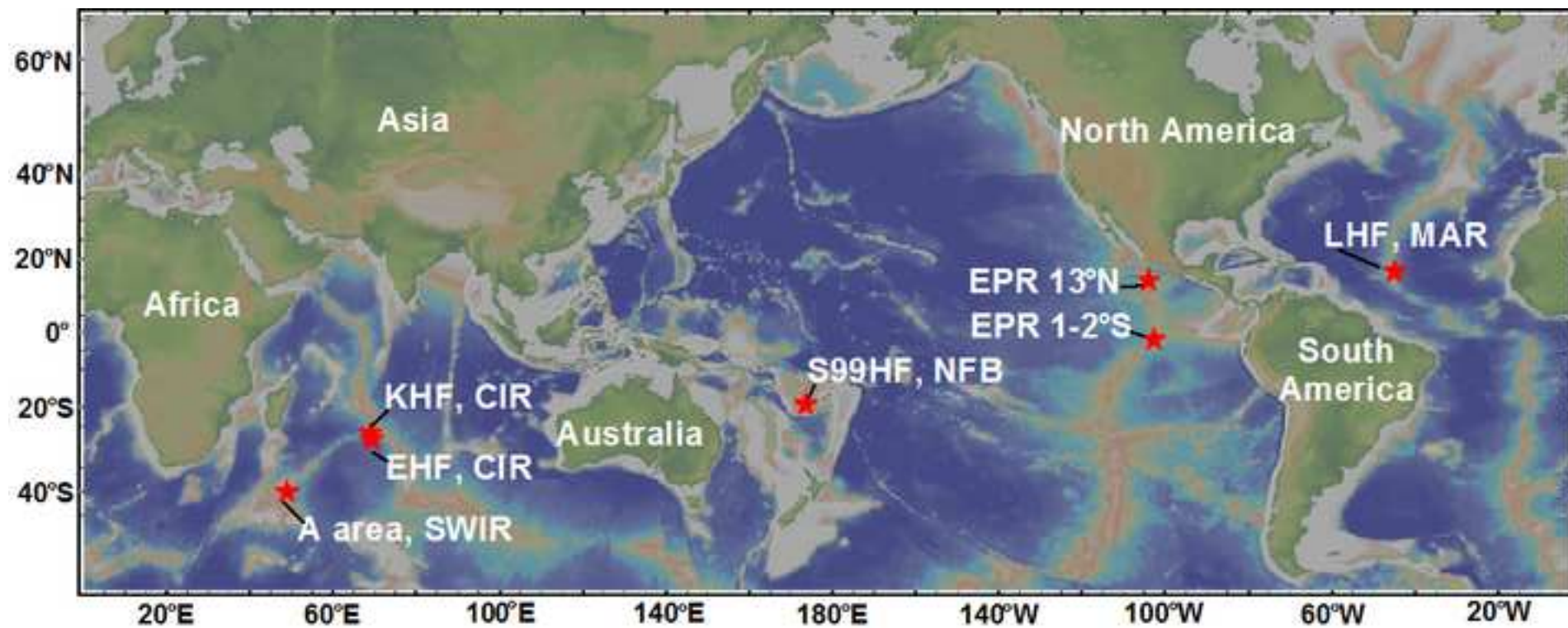


Figure 2
[Click here to download high resolution image](#)

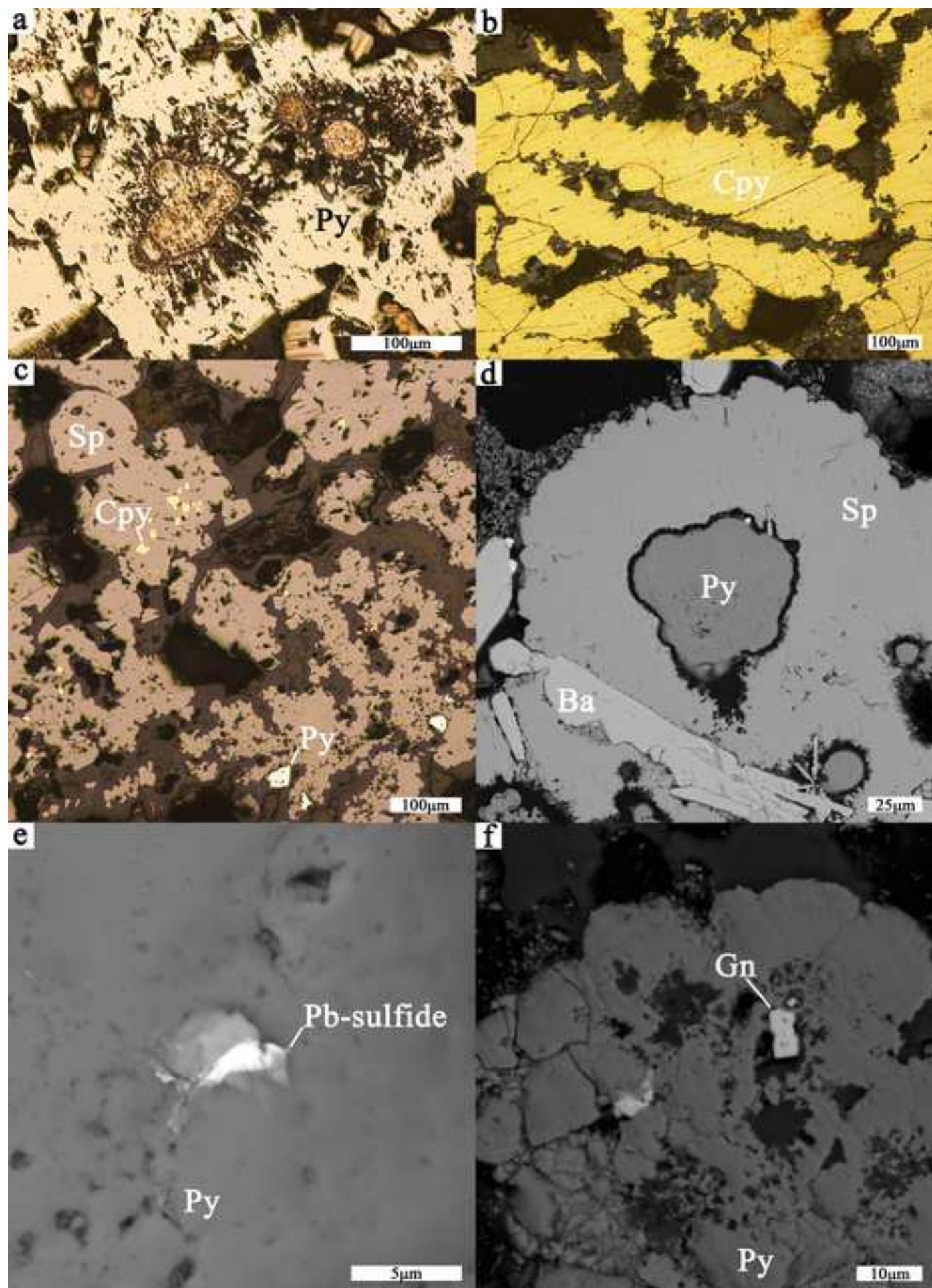


Figure 3
[Click here to download high resolution image](#)

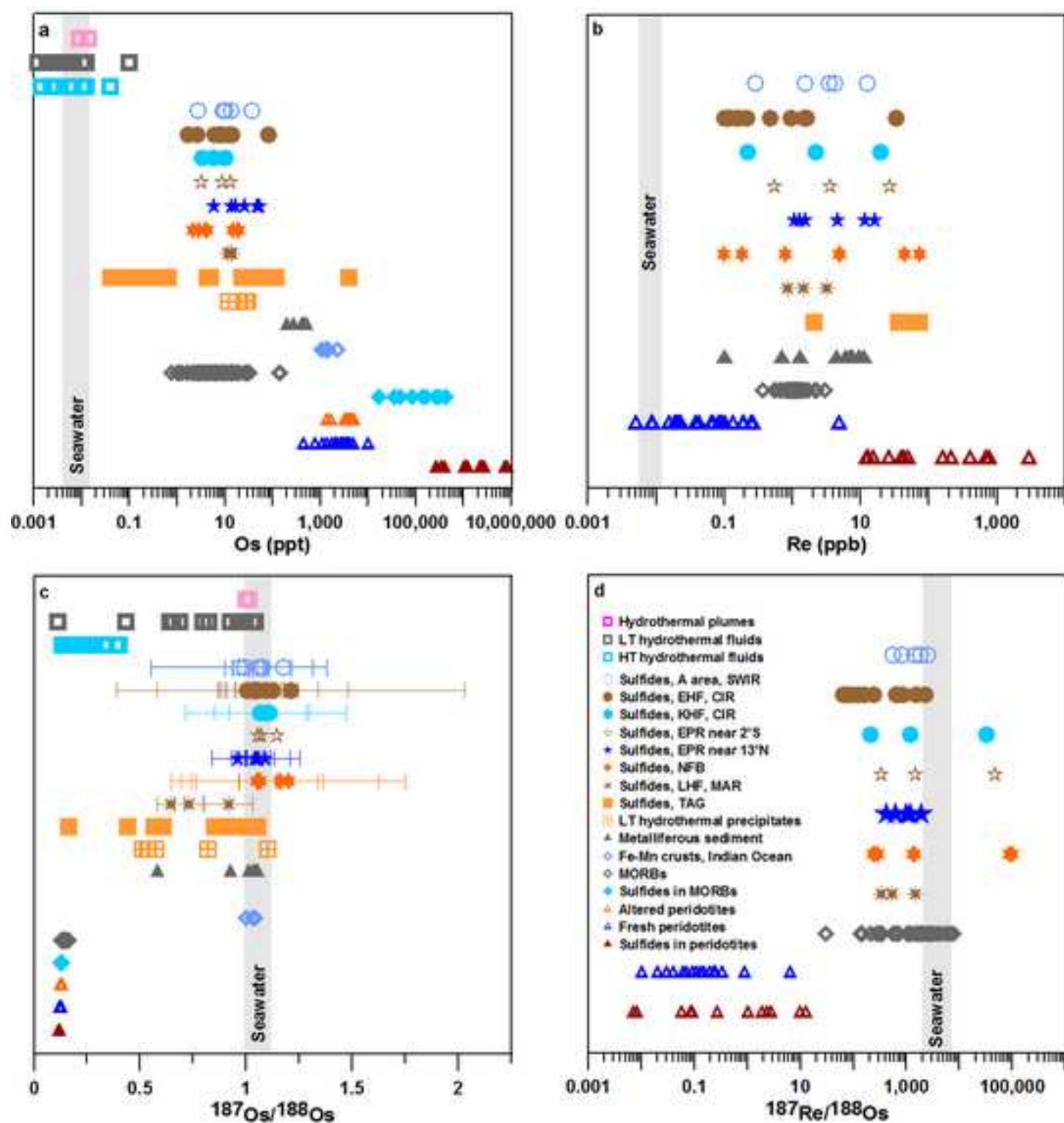


Figure 4
[Click here to download high resolution image](#)

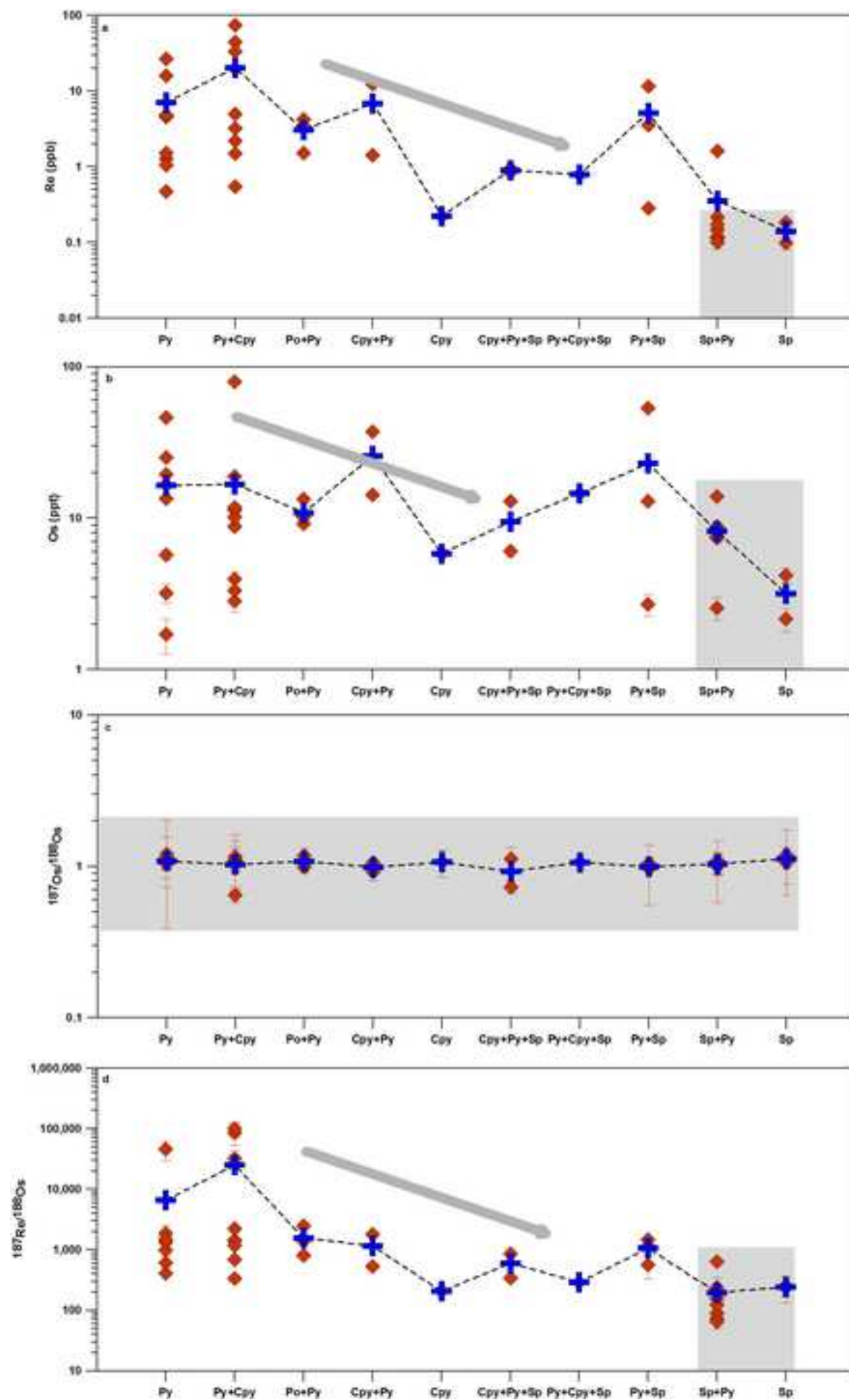


Figure 5
[Click here to download high resolution image](#)

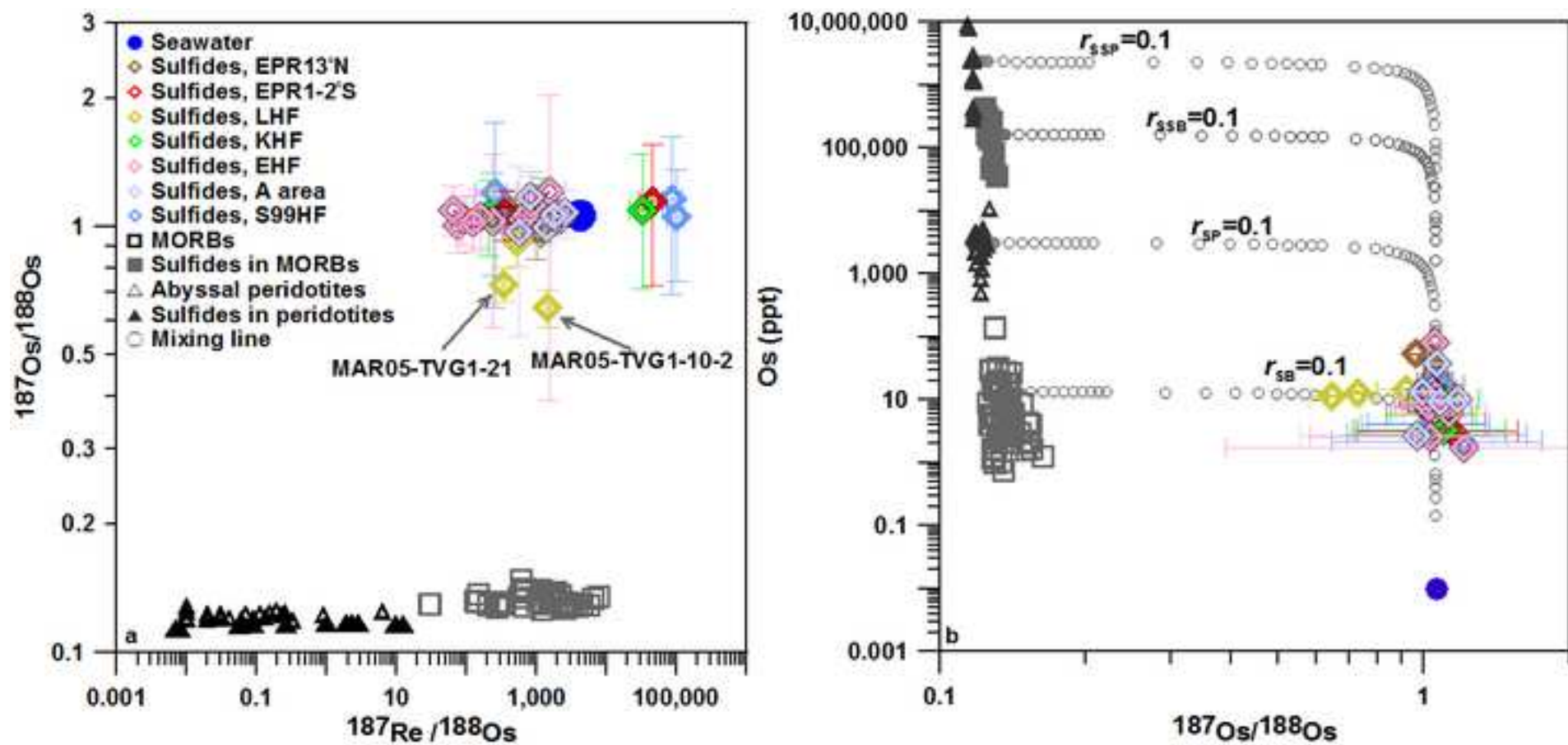


Figure 6
[Click here to download high resolution image](#)

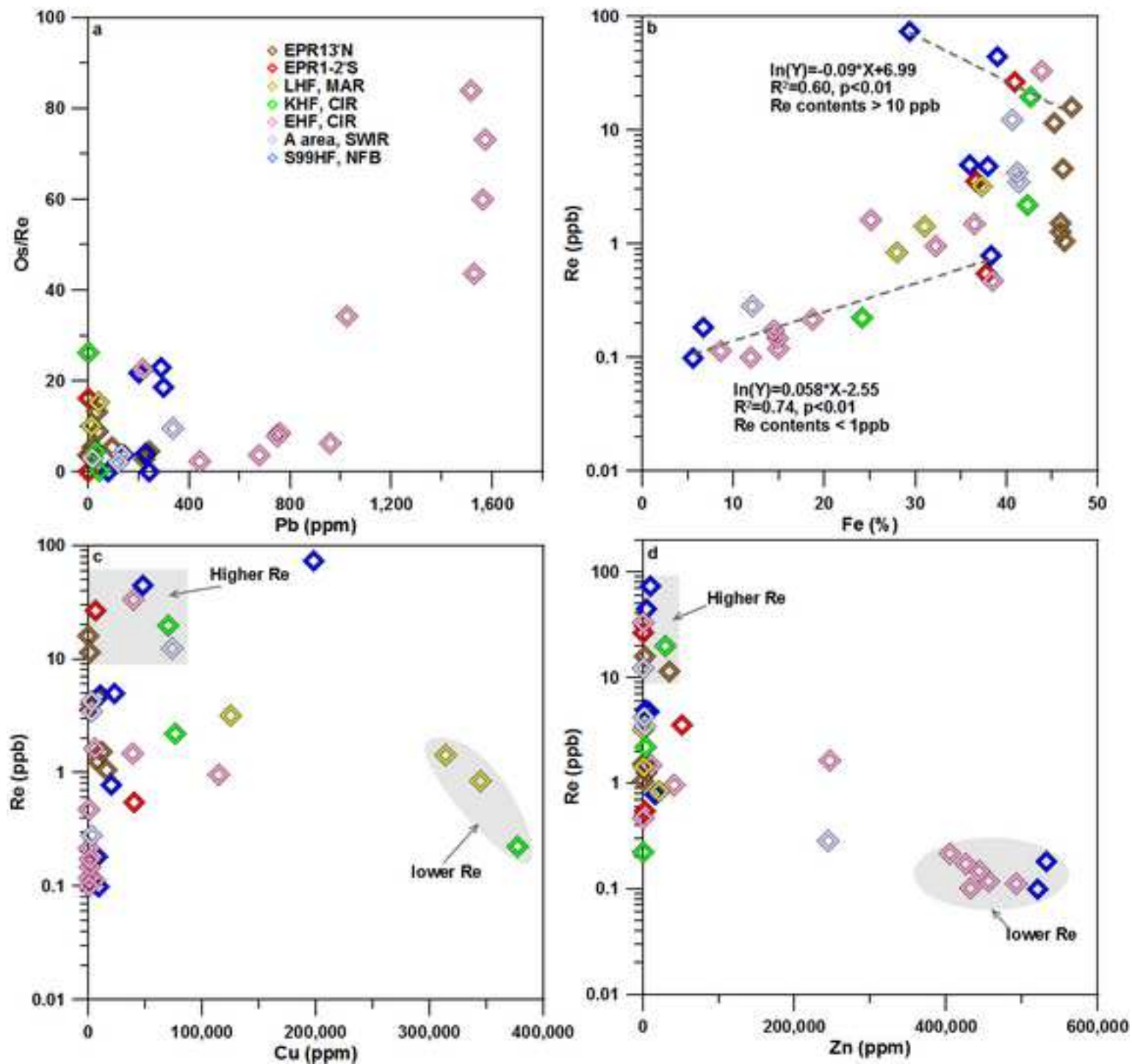


Table 1
Click here to download Table: Table 1.doc

Table 1 Description of seafloor massive sulfide samples.						
Field	Sample No.	Latitude	Longitude	Water depth (m)	Description	Sulfide mineralogy
Fast-spreading mid-ocean ridge						
13°N, EPR	EPR05-TVG1-2	12°42.669´N	103°54.426´W	2,628	Fe-rich massive sulfides coated with tan Fe hydroxides, and small conduits	Py +++; Sp +, Cpy +
13°N, EPR	EPR05-TVG1-3	12°42.669´N	103°54.426´W	2,628	Fe-rich massive sulfides coated with tan Fe hydroxides, and oxidized pyrite aggregates	Py +++; Cpy +, Sp +
13°N, EPR	EPR05-TVG2-1	12°42.678´N	103°54.414´W	2,633	Fe-rich massive sulfides coated with tan Fe hydroxides and many elliptical cavities, showing development of mineral zoning	Py +++; Mc +++; Sp +
Super-fast spreading mid-ocean ridge						
1-2°S, EPR	20III-S4-TVG1-1	1°22.130´S	102°37.360´W	2,747	Porous chimney fragment coated with tan Fe hydroxides and partially filled conduits	Py+++; Mc+, Cpy+; Sp+
1-2°S, EPR	20III-S4-TVG1-2	1°22.130´S	102°37.360´W	2,747	Chimney fragment coated with tan Fe hydroxides	Py +++; Cpy ++; Mc ++; Sp+
1-2°S, EPR	20III-S6-TVG3	2°09.102´S	102°38.760´W	2,921	Outer chimney wall fragment coated with red brown Fe hydroxides and white anhydrite layer	Mc +++; Py +++; Sp ++; Cpy +
Slow-spreading mid-ocean ridge						
LHF, MAR	MAR05-TVG1-9	14°45.186´N	44°58.772´W	3,025	Porous Cu-rich massive sulfide	Cpy +++; Py ++
LHF, MAR	MAR05-TVG1-10	14°45.186´N	44°58.772´W	3,025	Fragment with gypsum, amorphous silica, disseminated marcasite and chalcopyrite	Cpy +++; Py ++
LHF, MAR	MAR05-TVG1-21	14°45.186´N	44°58.772´W	3,025	Cu-rich massive sulfides fragment with small cavities	Cpy +++; Sp +; Py+
Intermediate-spreading mid-ocean ridge						
KHF, CIR	IR05-TVG9	25°19.221´S	70°02.420´E	2,437	Chimney fragment with finely bladed chalcopyrite	Py +++; Cpy +
KHF, CIR	19III-S12-TVG6	25°09.228´S	70°04.482´E	2,443	Porous Cu-rich sulfide fragment with yellowish brown oxides in the cavities, local light green secondary Cu sulfides	Cpy +++
EHF, CIR	IR05-TVG12	23°52.678´S	69°35.808´E	3,293	Grey black Zn-rich massive sulfides coated with red to brown oxide crusts, nodular structure in the outside	Sp +++; Py ++, Mc ++
EHF, CIR	IR05-TVG13-4-1	23°52.684´S	69°35.795´E	3,292	Oxidized columnar chimney coated with red brown oxides,	Cpy +++; Mc++, Sp++,

					and fluid conduits	Py++
EHF, CIR	IR05-TVG13-9.1	23°52.684'S	69°35.795'E	3,292	Irregular crust consisted of red brown to yellowish green oxide, anhydrite and gypsum, with disseminated sulfides	Py+++
EHF, CIR	IR05-TVG13-9.2-1	23°52.684'S	69°35.795'E	3,292	Chimney fragment with red, brown and yellowish green mixture of oxide, anhydrite and gypsum	Mc+++; Cpy++, Sp ++, Py++
EHF, CIR	19III-S18-TVG9	23°52.638'S	69°35.850'E	3,282	Porous Fe-Cu rich sulfides with minor sulfates	Py+++; Mc++, Sp ++, Cpy++
<i>Super-slow spreading mid-ocean ridge</i>						
A area, SWIR	19II-S7-TVG4	37°47.004'S	49°28.176'E	2,781	Black porous massive sulfides	Sp +++; Py++; Cpy+
A area, SWIR	20V-S35-TVG17	37°46.812'S	49°38.886'E	2,783	Massive sulfide with dark brown oxide crust	Po++, Py++; Cpy+
A area, SWIR	21VII-TVG22	37°56.316'S	49°15.894'E	1,443	Fe-rich chimney fragment coated with grey amorphous silica, conduits partially in-filled with oxides	Cpy++++, Py++++; Mc+, Sp +
<i>Back-arc basin</i>						
S99HF, NFB	113.1GTV	16°57.322'S	173°54.970'E	1,967	Porous massive sulfide	Py++, Cpy++
S99HF, NFB	42GTV	16°57.533'S	173°54.978'E	1,975	Cu-rich chimney fragment with conduits	Cpy++++; Py++, Mc++
S99HF, NFB	26.1GTV	16°57.602'S	173°54.991'E	1,976	Inner Zn-rich chimney wall fragment with yellowish brown oxides	Sp +++; Mc+, Cpy+
S99HF, NFB	26.2GTV	16°57.602'S	173°54.991'E	1,976	Greyish Zn-rich chimney fragment with local honeycomb structure and coarse black sphalerite crystals	Sp +++; Mc+, Cpy+

Py-pyrite; Mc-marcasite; Cpy-chalcopyrite; **Sp**-sphalerite; Po-pyrrhotite. +++: abundant (>30%); ++: major (5-30%); +: minor (≤5%).

Table 2
Click here to download Table: Table 2.doc

Table 2 Re-Os isotopic compositions of seafloor massive sulfides.

Sample No.	Mineralogy	Re	±2σ	Os	±2σ	¹⁸⁷ Re/ ¹⁸⁸ Os	±2σ	¹⁸⁷ Os/ ¹⁸⁸ Os	±2σ	Initial ¹⁸⁷ Os/ ¹⁸⁸ Os	Fe	Cu	Zn	Pb
East Pacific Rise near 13°N														
EPR05-TVG1-2-1	Py	1.26	0.03	16.70	0.73	410.5	43.7	1.090	0.117	1.090	45.9	8169	4,170	35.1
EPR05-TVG1-2-5	Py	1.53	0.02	13.50	0.50	610.6	52.7	1.038	0.094	1.038	45.9	11,430	488	39.9
EPR05-TVG1-3-1	Py	4.59	0.02	25.11	0.55	987.6	46.9	1.057	0.056	1.057	46.2	8,272	6,083	94.7
EPR05-TVG1-3-2	Py	1.05	0.02	5.74	0.44	990.6	187.1	1.046	0.209	1.046	46.4	15,935	141	17.0
EPR05-TVG2-1-1	Py	15.91	0.07	46.18	0.73	1,857.6	58.9	1.037	0.039	1.036	47.1	227	2,801	223.5
EPR05-TVG2-1-6	Py+Sp	11.54	0.04	53.36	0.78	1,155.6	33.3	0.961	0.034	0.961	45.2	1610	34,790	243.0
East Pacific Rise near 1-2°S														
20III-S4-TVG1-1-1	Py	26.80	0.09	3.21	0.45	45,589.5	16,091.1	1.143	0.416	1.141	40.9	5,958	865	1.15
20III-S4-TVG1-2-1	Py+Cpy	0.55	0.02	8.85	0.48	334.0	45.0	1.070	0.145	1.070	37.8	40,054	2,334	0.80
20III-S6-TVG3	Py+Sp	3.54	0.02	12.95	0.49	1,475.2	129.8	1.054	0.098	1.054	36.6	1,393	51,142	0.70
Logatchev hydrothermal field, MAR														
MAR05-TVG1-10-2	Py+Cpy	3.20	0.02	11.35	0.45	1,450.3	133.4	0.645	0.066	0.645	37.3	125,219	267	13.3
MAR05-TVG1-9	Cpy+Py	1.42	0.03	14.31	0.69	528.7	60.7	0.917	0.114	0.917	31.0	314,180	1,422	14.7
MAR05-TVG1-21	Cpy+Py+Sp	0.84	0.02	12.92	0.47	339.5	29.2	0.730	0.066	0.730	27.9	344,227	20,820	41.4
Kairei hydrothermal field, CIR														
IR05-TVG9-1	Py+Cpy	2.21	0.03	10.22	0.69	1,174.5	193.1	1.109	0.189	1.109	42.3	76,665	3,054	27.9
IR05-TVG9-3	Py+Cpy	19.78	0.07	3.31	0.45	32,379.8	10,888.0	1.093	0.380	1.092	42.7	70,004	30,130	45.9
19III-S12-TVG6	Cpy	0.22	0.02	5.84	0.46	206.3	44.4	1.067	0.215	1.067	24.1	376,988	801	1.54
Edmond hydrothermal field, CIR														
IR05-TVG12-5-4	Sp+Py	0.11	0.02	2.56	0.43	237.7	108.3	1.029	0.450	1.029	8.61	5,560	492,389	216
IR05-TVG12-8-2	Sp+Py	1.63	0.02	13.96	0.49	629.8	52.0	1.041	0.090	1.041	25.1	5,287	246,400	758

IR05-TVG12-8-3	Sp+Py	0.22	0.02	7.40	0.46	157.9	28.1	1.052	0.167	1.052	18.6	854	405,000	1,024
IR05-TVG12-9-1	Sp+Py	0.12	0.02	8.68	0.47	73.4	15.9	1.004	0.138	1.004	14.9	912	455,500	1,571
IR05-TVG12-11	Sp+Py	0.15	0.02	8.84	0.46	90.0	16.6	1.038	0.137	1.038	14.9	1,010	443,500	1,560
IR05-TVG12-12	Sp+Py	0.17	0.02	7.58	0.45	123.3	22.4	1.025	0.153	1.025	14.4	1,058	425,900	1,528
IR05-TVG12-14	Sp+Py	0.1	0.0	8.4	0.5	64.7	15.2	1.094	0.149	1.094	11.9	938	432,404	1,515
IR05-TVG13-4-1	Cpy+Py+Sp	1.0	0.0	6.0	0.5	861.2	159.5	1.125	0.215	1.125	32.2	114,193	40,755	959
IR05-TVG13-9.1	Py	0.5	0.0	1.7	0.4	1,514.3	1,002.3	1.209	0.820	1.209	38.4	803	270	677
IR05-TVG13-9.2-1	Py+Cpy	1.5	0.0	11.8	0.5	684.0	65.1	1.058	0.105	1.058	36.4	39,067	10,404	748
19III-S18-TVG9	Py+Cpy	33.5	0.1	79.9	1.1	2,264.0	56.2	1.048	0.034	1.048	43.8	39,713	332	442
<i>A area, SWIR</i>														
19II-S7-TVG4	Py+Sp	0.3	0.0	2.7	0.4	560.6	233.2	0.968	0.413	0.968	12.0	2,575	244,281	337
20V-S35-TVG17-3-2	Po+Py	3.5	0.0	13.3	0.5	1,399.0	120.1	0.993	0.090	0.993	41.3	2,637	2,480	134
20V-S35-TVG17-4-2	Po+Py	4.2	0.0	9.2	0.5	2,494.5	307.6	1.076	0.140	1.076	41.1	2,580	1,386	121
20V-S35-TVG17-7	Po+Py	1.5	0.0	10.2	0.5	813.9	93.1	1.174	0.140	1.174	n.a.	n.a.	n.a.	n.a.
21VII-TVG22	Cpy+Py	12.4	0.0	37.3	0.7	1,792.4	64.7	1.061	0.045	1.061	40.6	73,348	515	17.4
<i>Sonne 99 hydrothermal field, North Fiji Basin,</i>														
<i>BAB</i>														
113.1GTV-1	Py	4.79	0.03	19.46	0.61	1,330.4	93.8	1.053	0.087	1.053	37.9	10,357	7,875	227
113.1GTV-2	Py+Cpy	4.97	0.03	18.84	0.60	1,426.3	102.8	1.057	0.089	1.057	36.0	22,903	3,734	143
42GTV-1	Py+Cpy	44.45	0.15	2.83	0.44	85,800.7	33,324.5	1.160	0.466	1.157	39.0	48,071	5,146	240
42GTV-3	Py+Cpy	73.60	0.25	3.96	0.45	100,334.7	28,260.7	1.052	0.310	1.049	29.3	197,581	10,239	78.4
113.2GTV	Py+Cpy+Sp	0.79	0.02	14.61	0.54	291.1	25.8	1.066	0.102	1.066	38.3	20,238	15,960	297
26.1GTV-1	Sp	0.10	0.02	2.15	0.38	252.1	120.7	1.197	0.551	1.197	5.51	8,896	520,500	200
26.2GTV-1	Sp	0.18	0.02	4.21	0.45	234.0	66.1	1.051	0.287	1.051	6.64	7,882	531,900	289

Py-Fe sulfide, including pyrite and marcasite; Cpy-chalcopyrite; Sp-Zn sulfide, including sphalerite and wurtzite; Po-pyrrhotite. Unit ppb for Re; ppt for Os; % for Fe; ppm for Cu, Zn and Pb; n.a. not analyzed. Initial ¹⁸⁷Os/¹⁸⁸Os composition has been calculated at 2 ka.